Superconductivity at 9 K in Mo_5PB_2 with evidence for multiple gaps

Michael A. McGuire* and David S. Parker

Materials Science and Technology Division, Oak Ridge National Laboratory, Oak Ridge, Tennessee 37831, USA

(Received 1 December 2015; revised manuscript received 25 January 2016; published 9 February 2016)

Superconductivity is observed with critical temperatures near 9 K in the tetragonal compound Mo_5PB_2. This material adopts the Cr_5B_3 structure type common to superconducting $Nb_5Si_{3-x}B_x$, Mo_5SiB_2, and W_5SiB_2, which have critical temperatures of 5.8–7.8 K. We have synthesized polycrystalline samples of the compound, made measurements of electrical resistivity, magnetic susceptibility, and heat capacity, and performed first-principles electronic structure calculations. The highest T_c value (9.2 K) occurs in slightly phosphorus rich samples, with composition near $Mo_5P_{1.1}B_{1.9}$, and the upper critical field H_{c2} at $T = 0$ is estimated to be ≈17 kOe. Together, the measurements and band-structure calculations indicate intermediate coupling ($\lambda = 1.0$), phonon mediated superconductivity. The temperature dependence of the heat capacity and upper critical field H_{c2} below T_c suggest multiple superconducting gaps may be present.

DOI: 10.1103/PhysRevB.93.064507

I. INTRODUCTION

The tetragonal Cr_5B_3 structure type is adopted by a wide variety of binary and ternary compounds with examples incorporating at least 47 different elements spanning the main group, transitions metals, and rare-earth metals [1]. One of the more interesting subsets of these compounds is the ternary borides with stoichiometries M_5XB_2, with X = P,Si. These are reported to form with many transition metals (M) including the 3*d* transition metals from V to Co, the 4*d* transition metals Nb and Mo, and the 5*d* transition metal W. Mn_5SiB_2 and Mn_5PB_2 are ferromagnets with Curie temperatures near room temperature and are of interest for magnetocaloric applications [2,3]. Fe_5SiB_2 and Fe_5PB_2 are uniaxial ferromagnets with high Curie temperatures, and a low temperature spin reorientation in the case of the silicide, and have been studied as potential permanent magnet materials [4–7]. In striking contrast to these high-temperature ferromagnets, the 4*d* and 5*d* compounds Nb_5SiB_2, Mo_5SiB_2, and W_5SiB_2 are superconductors with transition temperatures of 7.2, 5.8, and 5.8 K, respectively [8–10]. The occurrence of superconductivity in these borosilicide compounds brings to mind other well-known boron-containing, phonon-mediated superconductors, including the borocarbides RT_2B_2C (R = rare-earth element, T = Ni, Pd, Pt) [11] and magnesium diboride MgB_2 [12].

The observation of superconductivity in several examples of Cr_5B_3-type compounds with the 512 stoichiometry suggests that further examination may produce more examples in this relatively new group of superconductors [9]. In the present work, we have studied the analogous Mo_5PB_2, and find that it too is a superconductor. The superconducting critical temperature (T_c) is determined to be as high as 9.2 K. This is the highest T_c yet reported for superconductors in this structure type. In addition to measurements of resistivity, magnetic susceptibility, and heat capacity, we report results of first-principles calculations that reveal the presence of multiple bands crossing the Fermi level in this borophosphide and the related borosilicides, as seen in, for example, the iron-based superconductors including the phosphide LaFePO [13], as well as MgB_2 [14]. Calculations indicate the coupling in Mo_5PB_2 is in the intermediate limit (i.e., the electron-phonon coupling $\lambda \approx 1$). Analysis of the heat-capacity and upper critical field data suggests the presence of two distinct energy gaps. Together the experimental and theoretical results indicate that Mo_5PB_2 may be a multiband superconductor.

II. PROCEDURES

Polycrystalline samples with nominal compositions $Mo_5P_{0.9}B_{2.1}$, Mo_5PB_2, and $Mo_5P_{1.1}B_{1.9}$ were prepared from hydrogen-reduced molybdenum powder (99.999%), phosphorus pieces (99.999%), and boron powder (99.5%). The elements were reacted together at 1050 °C for 16–24 h, and the resulting powders were pressed into cylindrical pellets and heated at 1100–1150 °C for a total duration of up to eight days, with intermediate grinding and repelletizing. Crystals of the isostructural Fe_5PB_2 have been grown from an Fe-P melt [7], however, there is no liquid region on the Mo-rich side of the Mo-P phase diagram below about 1700 °C. The optical floating-zone method has been used to grow crystals of Mo_5SiB_2 [15], however, arc-melting experiments in our lab indicate that Mo_5PB_2 does not melt congruently, and the volatility of phosphorus may preclude this type of crystal growth. The most likely route to single crystal Mo_5PB_2 may be the molten metal flux technique [16,17], if a suitable flux can be identified.

Powder x-ray diffraction was performed using monochromatic Cu $K_{\alpha 1}$ radiation with a PANalytical X'Pert Pro diffractometer and analyzed using the Rietveld technique with the FULLPROF software package [18]. Magnetization measurements were performed with a Quantum Design magnetic property measurement system (MPMS) and physical property measurement system (PPMS). The PPMS was also used for measurements of electrical resistivity and heat capacity. The heat-capacity data were analyzed using both the conventional relaxation method employing small heat pulses (temperature rise of 2% of the sample temperature) and slope-analysis [19] of large heat pulse data (temperature rise of 30% of the sample temperature).

First-principles density functional theory calculations of the electronic structure of Mo_5PB_2 were performed using

*McGuireMA@ornl.gov

the linearized augmented plane-wave (LAPW) code WIEN2K [20], employing the generalized gradient approximation of Perdew, Burke, and Ernzerhof [21]. LAPW sphere radii of 2.41, 2.08, and 1.7 bohrs, respectively for Mo, P, and B were chosen with an RK_{max} of 7.0, where RK_{max} is the product of the smallest sphere radius and the largest plane-wave expansion wave vector. Internal coordinates were relaxed until forces on the ions were less than 2 mRy/bohr.

III. RESULTS AND DISCUSSION

Rietveld analysis showed the resulting purity of the samples to be 92, 89, and 92% by weight for samples with nominal compositions $Mo_5P_{0.9}B_{2.1}$, Mo_5PB_2, and $Mo_5P_{1.1}B_{1.9}$, respectively. Mo_3P and MoB were observed as impurity phases in all samples. Refinement results are shown for $Mo_5P_{1.1}B_{1.9}$ in Fig. 1(a), where the crystal structure is shown in the inset.

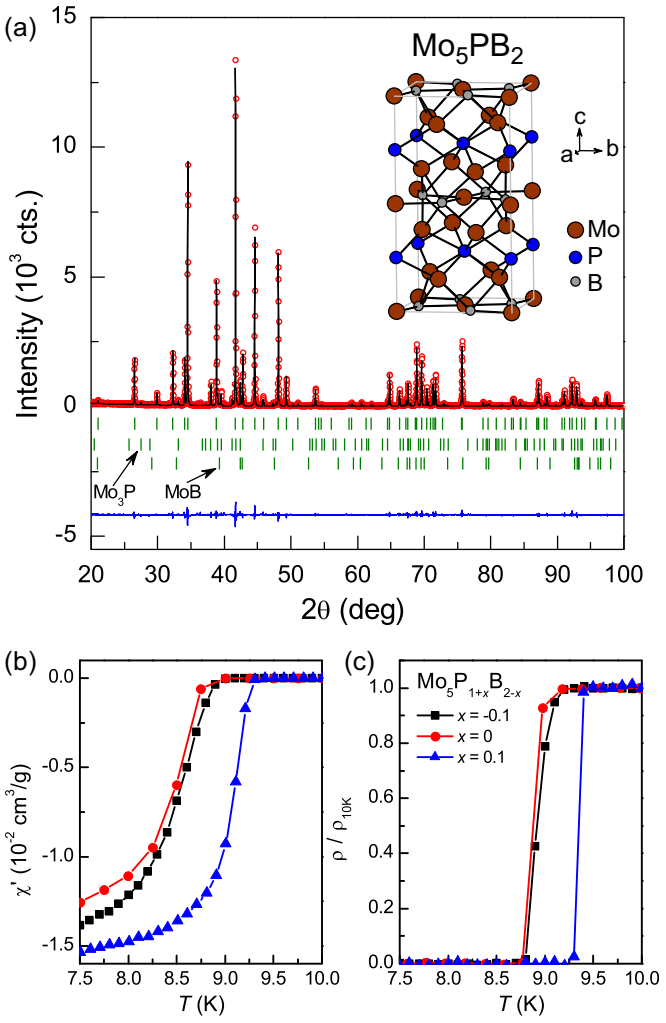

FIG. 1. The crystal structure of Mo_5PB_2 is shown in (a) along with results of Rietveld refinement of powder x-ray-diffraction data from a sample with nominal composition $Mo_5P_{1.1}B_{1.9}$. The ticks locate Bragg reflections from the main phase (92% by weight) and the Mo_3P and MoB impurity phases. Variation of T_c with nominal composition is demonstrated in (b) and (c), which show magnetic susceptibility and resistivity data, respectively.

Table I contains the refined crystallographic properties of the Mo_5PB_2 phase in each sample. Allowing mixed occupation of P and B on their respective sites suggested some P may reside on the B site, but did not indicate any mixing of B onto the P site. The compositions determined from the refined occupancies are listed in the table. Adding excess P (relative to Mo_5PB_2) appears to significantly increase the P content of the main phase, as indicated by both the refined composition as well as the increase in the unit-cell volume. Addition of excess B had no detectable effect on the atomic site occupancies (relative to Mo_5PB_2) and produced only a small decrease in the unit-cell volume. These observations indicate that there is some phase width in Mo_5PB_2 with respect to the P and B ratio, a common feature in this structure type [7,8,22–24], and that in this case excess P is favored.

Figures 1(b) and 1(c) show the ac magnetic susceptibility and resistivity measured below 10 K. All of the samples are superconducting. Values of T_c are determined by the onset of diamagnetism [Fig. 1(b)] and the temperature at which the resistivity reaches zero [Fig. 1(c)]. These are listed for each sample in Table I. Similar values of $T_c = 8.7$–8.9 K are seen in the $Mo_5P_{0.9}B_{2.1}$ and Mo_5PB_2 samples, which have similar stoichiometries as discussed above. A higher value of $T_c = 9.2$ K is seen in $Mo_5P_{1.1}B_{1.9}$. This demonstrates the sensitivity of the superconductivity to the chemical composition of the Mo_5PB_2 phase. Further experimental analysis presented here will focus primarily on the $Mo_5P_{1.1}B_{1.9}$ sample. The T_c values seen in these materials are the highest yet reported in this class of ternary superconductors, which include Mo_5SiB_2 ($T_c = 5.8$ K) [9], Nb_5SiB_2 ($T_c = 7.2$ K) [9], W_5SiB_2 ($T_c = 5.8$ K) [10], $W_{5-x}Ta_xSiB_2$ ($T_c = 6.5$ K) [25], and the closely related $Nb_5Si_{2.4}B_{0.6}$ ($T_c = 7.8$ K) [22].

Figure 2 shows the results of magnetization measurements on $Mo_5P_{1.1}B_{1.9}$. The dc measurements were conducted in 10 Oe field, and the ac magnetization measurements were conducted in a dc field of 10 Oe using a frequency of 1 kHz and an ac excitation field of 5 Oe. The superconducting transition is marked by the onset of diamagnetism in the dc susceptibility (χ_{dc}) and the real part of the ac susceptibility (χ'), while the imaginary part (χ'') peaks just below T_c. The large diamagnetic signal in both field-cooled (fc) and zero-field-cooled (zfc) measurements demonstrates the bulk nature of the superconductivity. Complete magnetic-flux exclusion corresponds to a volume susceptibility of $-1/4\pi$ in the units used here. This corresponds to a mass susceptibility of 0.0089 cm^3/g using the single-crystal density of 8.97 g/cm^3 determined from the structure refinements presented above. Thus, the shielding fraction indicated by the data in Fig. 2(a) exceeds unity by almost a factor of 2. This may be attributed to geometrical and demagnetization effects in these samples, which were loosely compacted powders in irregular shapes. A shielding volume fraction of 120% was observed (with no demagnetization correction) for a denser sample that was cold pressed at high pressure between tungsten carbide anvils.

Resistivity data for polycrystalline $Mo_5P_{1.1}B_{1.9}$ are shown in Fig. 3. The residual resistivity ratio is $\rho_{2K}^{2T}/\rho_{300K} = 11$, relatively high considering the polycrystalline nature of the sample. The resistivity varies like $T^{2.4}$ above T_c up to about 60 K. Above about 100 K, $\rho(T)$ displays a negative curvature rather than the linear behavior expected for most metals.

TABLE I. Results of room-temperature x-ray-diffraction analysis [space group $I4/mcm$, Mo1 at (0,0,0), Mo2 at (x_{Mo2},$x_{Mo2}+\frac{1}{2}$,z_{Mo2}), P at (0,0,$\frac{1}{4}$), B at (x_B,$x_B-\frac{1}{2}$,0)] and measured superconducting transition temperatures.

Nominal comp.	$Mo_5P_{0.9}B_{2.1}$	Mo_5PB_2	$Mo_5P_{1.1}B_{1.9}$
Refined comp.	$Mo_5P_{1.07(4)}B_{1.93(4)}$	$Mo_5P_{1.07(4)}B_{1.93(4)}$	$Mo_5P_{1.12(3)}B_{1.88(3)}$
a (Å)	5.9726(1)	5.97303(7)	5.97633(6)
c (Å)	11.074(3)	11.076(1)	11.0813(2)
V (Å^3)	395.04(2)	395.142(7)	395.784(8)
x_{Mo2}	0.1663(3)	0.1659(3)	0.1661(2)
z_{Mo2}	0.1409(2)	0.1410(2)	0.1409(2)
x_B	0.619(5)	0.618(4)	0.620(3)
$T_c^{\rho=0}$ (K)	8.7(1)	8.8(2)	9.2(1)
$T_c^{\chi'\text{onset}}$ (K)	8.9(1)	8.7(2)	9.2(1)

The normal-state temperature dependence is similar to that reported for Mo_5SiB_2 [9] and W_5SiB_2 [10], and the negative curvature at higher temperatures has been observed as a common feature in a variety of chemically related compounds, based on Mo_5X_3 (x = Si, B, C) [26]. This behavior is also seen in the $A15$-type superconductors, where Fisk and Webb concluded that resistivity saturation results from the approach to the Mott-Ioffe-Regel limit [27]. This occurs when the electron mean free path reaches a minimum value defined by the lattice constant [28,29]. Gurvitch [30] cast the resulting relationship between the saturation resistivity ρ_{sat} in $\mu\Omega$ cm, the carrier concentration n in cm^{-3}, and lattice parameter a in Å (assuming cubic symmetry) into the following useful form: $\rho_{sat} = 1.29 \times 10^{18}/(n^{2/3}a)$ $\mu\Omega$ cm. Hall effect measurements on $Mo_5P_{1.1}B_{1.9}$ give a Hall coefficient of $R_H \approx -3.1 \times 10^{-4}$ cm^3/C. From this, in a simple one-band model, a carrier concentration of 2×10^{22} electrons per cm^3 is inferred. Using this value of n and the average lattice constant of $(2a + c)/3 = 7.7$ Å gives $\rho_{sat} = 230$ $\mu\Omega$ cm. The resistivity data in Fig. 3 exceed this value by about 60% at room temperature, which may be attributed to the polycrystalline nature of the sample with resistive grain boundaries. However, this estimated ρ_{sat} does compare well with data reported for several isostructural M_5SiB_2 compounds that have been measured up to 1000 K [26].

Resistivity data collected in applied magnetic fields are shown in the upper inset of Fig. 3. In zero field the resistive transition is very sharp, with a width of $\lesssim 0.1$ K. The transition broadens as magnetic field is applied, with the width increasing to 0.7 K at 12.5 kOe. This is typical behavior of a type-II superconductor. From the resistivity data, the field dependence of T_c is obtained, where T_c is defined as the temperature

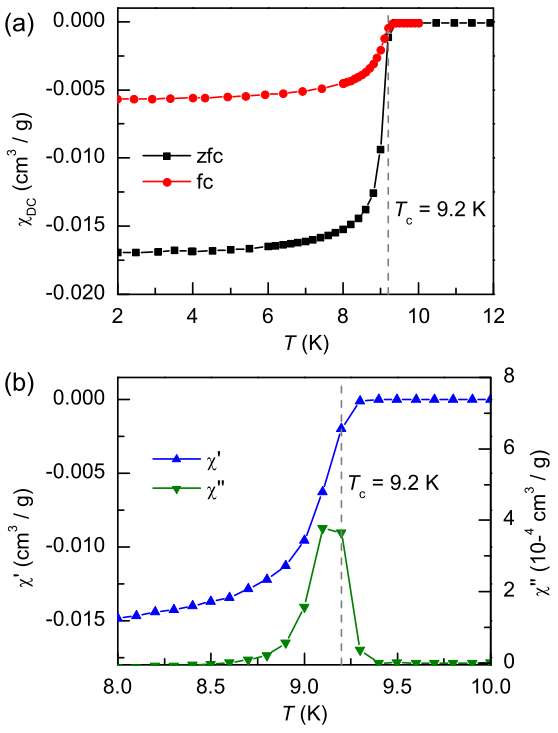

FIG. 2. Results from (a) dc and (b) ac magnetization measurements on $Mo_5P_{1.1}B_{1.9}$. The dc data show both zero-field-cooled (zfc) and field-cooled (fc) results. The ac data were collected in zfc mode and both the real (χ') and imaginary (χ'') parts of the ac susceptibility are shown. The superconducting transition temperature T_c determined by the onset of diamagnetism is indicated by the dashed line.

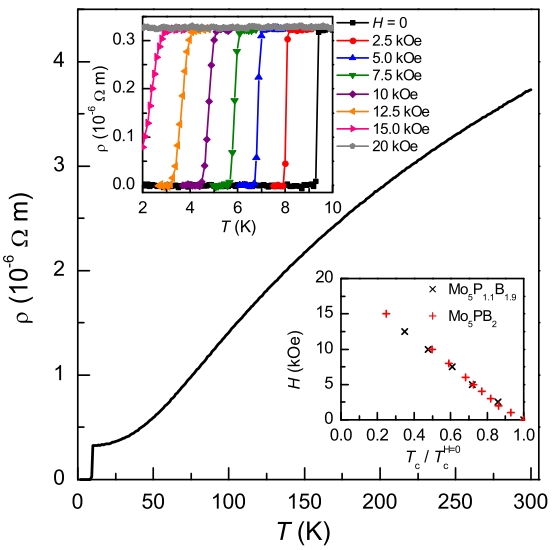

FIG. 3. Resistivity of $Mo_5P_{1.1}B_{1.9}$ in zero applied magnetic field is shown in the main panel. The upper inset shows the effect of magnetic field on T_c, which is plotted in the lower inset. The lower inset also includes data from the Mo_5PB_2 sample for comparison.

at which $\rho \to 0$. The results are shown in the lower inset of Fig. 3, which also include results from the same analysis applied to the sample of nominal composition Mo_5PB_2. From these data, an upper critical field $H_{c2}(0)$ of ≈17 kOe can be estimated. This is significantly larger than in the closely related superconductors Mo_5SiB_2 and W_5SiB_2, for which values of 6 and 5 kOe, respectively, are reported [9,10]. Nearly linear behavior, with a slight positive curvature near $H = 0$, is observed up to fields of 12.5 kOe in Fig. 3. Fitting this range gives a slope of −2.1 kOe/T. From this value, the WHH expression $H_{c2}(0) = -0.693 T_c (dH_{c2}/dT)|_{T=T_c}$ gives $H_{c2}(0) = 13$ kOe. This is not compatible with the resistivity data collected at $H = 15$ kOe (Fig. 3), for which $T_c \approx 1.5$ K can be estimated (Fig. 3). This discrepancy is a direct result of the nearly linear relationship between magnetic field and T_c over a wide range of fields. A similar shape of H_{c2} vs T_c is seen in W_5SiB_2 [10], but reports for Mo_5SiB_2 show clear negative curvature over most of the temperature range [9], more consistent with expectations based on the WHH theory. The observed temperature dependence of the upper critical field H_{c2} in polycrystalline Mo_5PB_2 may be an indication of contributions from multiple superconducting gaps arising from underlying crystalline anisotropy or from multiple superconducting bands. Similar shapes have been observed in several multigap superconductors including polycrystalline MgB_2 [31] and $LaFeAsO_{0.89}F_{0.11}$ [32], and single crystals of borocarbides [33], dichalcogenides [34,35], and more recently $TlNi_2Se_2$ [36].

Results of heat-capacity measurements on $Mo_5P_{1.1}B_{1.9}$ are shown in Fig. 4. Rietveld refinement of the powder x-ray-diffraction data shows that this sample contains 7 wt % of Mo_3P, which is a superconductor with T_c reported of 5–7 K [37–39]. For this study, an Mo_3P sample was synthesized and its heat capacity was measured and subtracted from the total heat capacity measured for the $Mo_5P_{1.1}B_{1.9}$ sample after scaling by the x-ray-diffraction determined concentration. The measured T_c for the Mo_3P sample was 5.5 K. See the Appendix for additional data and information.

At 300 K the heat capacity of $Mo_5P_{1.1}B_{1.9}$ reaches 86% of the Dulong-Petit limit [Fig. 4(a), inset]. The increase in heat capacity upon cooling into the superconducting state is centered at $T_c = 9.2$ K. The magnitude of the heat-capacity jump is determined to be 43.2 mJ/mol at./K. Data collected at 30 kOe show that this field is sufficient to suppress the superconductivity to below 2 K, consistent with the resistivity results above that show $H_{c2}(0) \approx 17$ kOe. Figure 4(b) shows the electronic portion of the heat capacity, determined by subtracting the data collected at 30 kOe. The 30 kOe data are well described up to 9 K by $c_P(T) = \gamma T + \beta T^3$, as shown by the black line through the data in Fig. 4(a). This fit gives a normal-state Sommerfield coefficient of $\gamma = 3.16(1)$ mJ/mol at./K^2 and a Debye temperature of 492(2) K. Similar values were obtained from the same analysis of heat-capacity data (not shown) for the Mo_5PB_2 sample. These values are compared with other isostructural superconductors in Table II.

Results of electronic band-structure calculations are shown in Fig. 5(a). Six bands are observed to cross the Fermi level, with several bands contributing strongly to the the total density of states (DOS). The partial Fermi-level DOS in these bands

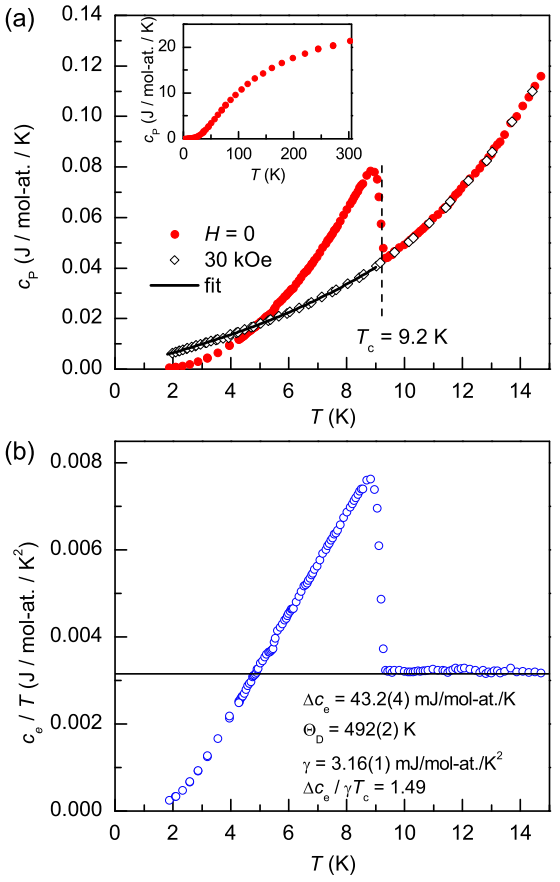

FIG. 4. Heat capacity of $Mo_5P_{1.1}B_{1.9}$, after correction for the 7 wt % Mo_3P impurity (see Appendix). The total heat capacity c_P is shown in (a), near T_c in the main panel and up to 300 K in the inset. The electronic component of the heat capacity determined by subtracting data collected at $H = 30$ kOe from data taken in zero field is shown in (b) plotted as c_e/T. The solid line in (b) is at $c_e/T = \gamma$.

(per unit cell per eV, both spins) is found to be 2.06, 4.66, 1.90, 1.10, 0.96, and 0.04, for a total Fermi level DOS $N(E_F)$ of 10.7 /eV/unit cell. With 10 Mo per unit cell and the majority of the DOS being Mo [Fig. 5(b)], $N(E_F)$ is somewhat enhanced relative to elemental Mo itself, which has $N(E_F)$ of 0.65 eV [40], but not to a degree that would suggest a magnetic instability. This argues in favor of a phononic pairing mechanism.

The value of γ determined from the calculated band structure [Fig. 5(a)] is 1.57 mJ/mol at./K^2. This is significantly lower than the observed value of 3.16 mJ/mol at./K^2. This

TABLE II. Results of heat-capacity analysis of superconducting 512-type materials.

Composition	$Mo_5P_{1.1}B_{1.9}$	Mo_5PB_2	Mo_5SiB_2 [9]	W_5SiB_2 [10]
T_c (K)	9.2	8.8	5.8	5.8
γ (mJ/mol at./K^2)	3.12	3.07	2.12	1.60
Θ_D (K)	494	501	515	470
Δc_e (mJ/mol at./K)	39.9	35	17.1	13.8
$\Delta c_e/(\gamma T_c)$	1.39	1.30	1.39	1.49

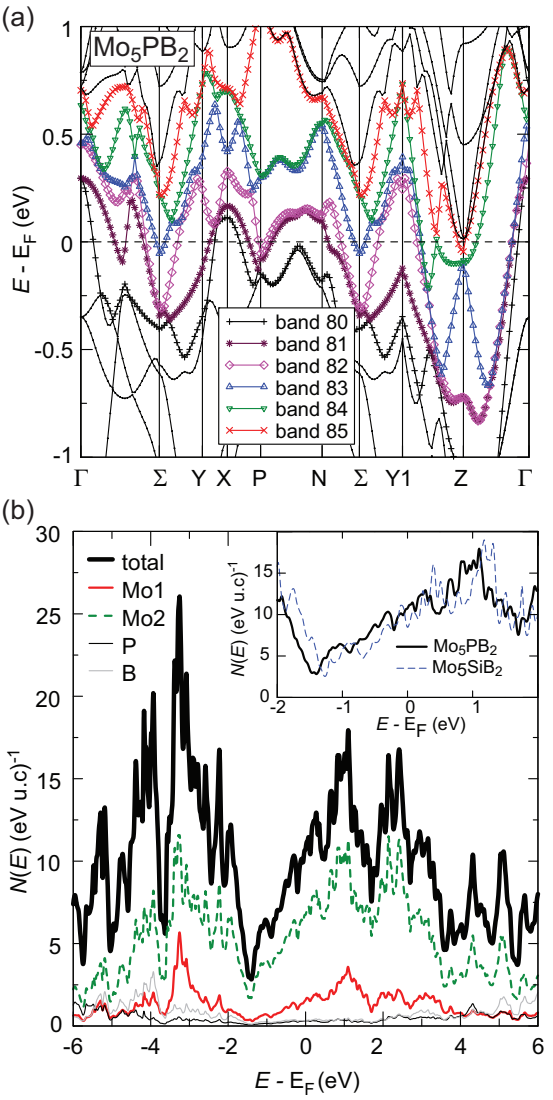

FIG. 5. Results of DFT calculations. (a) The calculated band structure of Mo_5PB_2. The six bands crossing the Fermi level are indicated by various symbols and labeled by numbers that enumerate the bands at each k point with respect to energy. (b) The calculated density of states per eV per unit cell of Mo_5PB_2, with an inset comparing the total density of states of Mo_5PB_2 with Mo_5SiB_2. The energy zero is set to the Fermi energies of the respective compounds.

enhancement by a factor of $2.01(=1+\lambda)$ gives an electron-phonon coupling constant λ of approximately 1, indicating intermediate coupling. For a single-band s-wave scenario, Eliashberg theory [41] gives a reduced specific-heat jump of approximately 2 for elemental Nb, which has a similar λ. The observed value of $\Delta c/\gamma T_c$ in Mo_5PB_2 is 1.49, close to the weak-coupling BCS value, but only 75% of the value expected based on the estimated electron-phonon coupling strength for this compound.

In general, such a reduced specific-heat jump can result from two factors. The first of these is gap anisotropy, including nodal behavior as observed in the superconducting cuprates [42] or more recently in LaFePO, a structural relative of the high T_c iron-based superconductors [43,44]. For example, the BCS weak-coupling theory, applied to a single band

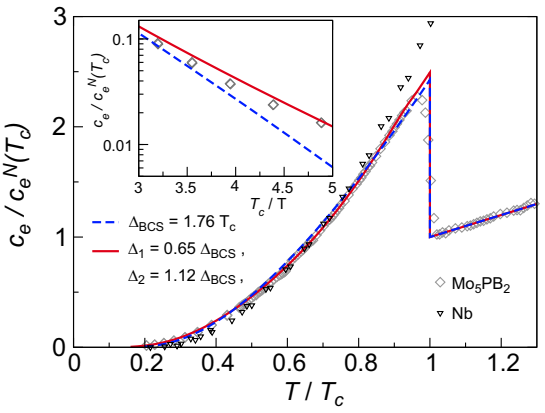

FIG. 6. The measured (grey diamonds) and calculated electronic specific heat of $Mo_5P_{1.1}B_{1.9}$ The dashed grey line indicates a single-band BCS weak-coupling calculation and the solid blue line the two band fit. Experimental data for Nb, a single gap superconductor with similar T_c, and λ are also shown for comparison (black triangles) [48]. Inset: the low-temperature specific-heat data and fits on a logarithmic scale.

two-dimensional d-wave material [45], predicts a reduced specific-heat jump $\Delta c/\gamma T_c$ of 0.95. However, there is little evidence for nodal superconductivity in Mo_5PB_2. For example, the electronic specific heat in the superconducting state in Fig. 4(b) at 1.9 K, or approximately 20 percent of T_c, is only 2% of the normal-state value at T_c, consistent with BCS predictions for a gapped s-wave superconductor.

The second possibility for such a reduced specific-heat jump is multiband superconductivity, as observed in MgB_2 [12]. Strictly speaking this can be considered a form of anisotropy, but here we follow the historical context and treat it separately from the Fermi-surface gap anisotropy described above. In MgB_2, well established to be an intermediate coupling multiband s-wave superconductor [46], the largest specific-heat jump $\Delta c/\gamma T_c$ was observed [47] to be 1.32, less than the BCS s-wave value. The band-structure calculations for Mo_5PB_2 support the possibility of multiband superconductivity, since several bands contribute significant DOS at the Fermi level.

Further evidence suggesting potential multiband behavior is seen in the temperature dependence of the heat capacity measured below T_c. In Fig. 6 we depict the heat-capacity data of Mo_5PB_2, along with two calculated curves: a single band BCS fit where the $T=0$ gap value has been taken as the canonical BCS weak-coupling value, $1.76k_BT_c$, and a two band fit with two gaps. The smaller gap is weighted at one-third the weight of the larger and the two gap fitting yields one gap of 0.65 times the BCS value and the other gap 1.12 times the BCS value. The relative weighting of the two band fit is in rough agreement with the highest two Fermi-level DOS values from the band-structure calculations.

Experimental data from Nb, which has a similar electron-phonon coupling λ as well as similar T_c, is included in Fig. 6 for comparison. The data were taken from Ref. [48]. If Mo_5PB_2 is a single band superconductor, as Nb is known to be, one would expect a similar electronic specific-heat curve. Instead, one finds a specific-heat jump $\Delta c/\gamma T_c$ only slightly above the weak-coupling BCS value. In addition, the low-temperature

specific heat is *enhanced* relative to the BCS value, as indicated in the inset. The low-T enhancement of the specific heat was found, in the case of MgB_2 [47], to result from having one gap much smaller than the BCS value. Often the specific heat at low temperature is taken to vary exponentially in $-\Delta/T$, where Δ is the smallest energy gap in the system, but the data (red diamonds) in the logarithmic plot in the inset of Fig. 6 show a substantial curvature demonstrating excitations across at least two gaps. The two band fit significantly improves upon the BCS fit, generating better agreement at both low temperatures and temperatures near T_c, though measurements on single crystals would be desirable to support this. This is consistent with the electronic structure calculations, finding multiple bands crossing E_F.

It is of interest to compare the experimental and theoretical results for Mo_5PB_2 to the isostructural compound Mo_5SiB_2, which is itself a superconductor with a somewhat lower T_c of 5.8 K [9]. From a comparison of our calculated γ of 1.22 mJ/mol atom K^2 for the Si compound with the γ of 2.12 mJ/mol atom K^2 measured in Ref. [9], an electron-phonon coupling constant $\lambda_{Mo_5SiB_2}$ of 0.73 is determined, significantly lower than the value of 1.0 we infer for the P compound. Given that the Debye temperatures of these two materials are quite similar, the lower value of λ for the Si compound immediately translates to a lower T_c.

Our calculations also provide insight into the source of this change in λ. Presented in the inset of Fig. 5(b) are the calculated total densities of states of the two compounds in a window of width approximately 4 eV, centered on E_F. It is apparent that the densities of states can nearly be superimposed upon each other in a "rigid-band" manner, with a shift of approximately 0.2 eV corresponding directly to the two fewer valence electrons of the Si compound. Since the calculated densities of states both generally increase with energy around the respective Fermi energies, the effective hole doping associated with the substitution of Si for P lowers the Fermi-level DOS. We note that this DOS reduction from 10.7 to 8.30 per eV per unit cel, or 22%, parallels the inferred 27% λ reduction from the P compound to the Si compound. This suggests that the electron phonon matrix element V [recalling that in BCS theory $\lambda = N(E_F)V$] is similar in the two compounds, as is reasonable. In addition, the calculations are consistent with the observation that the P-rich sample $Mo_5P_{1.1}B_{1.9}$ has a higher T_c than the Mo_5PB_2 sample (Table I), since the DOS at E_F [Fig. 5(b)] would be increased by the substitution of P for B.

Our first-principles calculations and analysis of the experimental data thus suggest that Mo_5PB_2 is an intermediate coupling, phonon-mediated, and potentially multiband superconductor. We note that it is possible that the superconductors Mo_5SiB_2 and additionally Nb_5SiB_2 are also multiband materials as our calculations (depicted in the Appendix) find each of these materials to have several bands crossing E_F.

IV. SUMMARY AND CONCLUSIONS

We have discovered a new superconductor, Mo_5PB_2, with critical temperature T_c as high as 9.2 K. It crystallizes in a tetragonal Cr_5B_3 structure shared by a number of superconductors, such as Mo_5SiB_2, Nb_5SiB_2, and W_5SiB_2, and has the highest transition temperature and upper critical field reported for this family of compounds. Electron doping may be expected to increase T_c further. Based on analysis of the specific-heat data as well as our first-principles calculations, Mo_5PB_2 appears to be an intermediate-coupling, multigap, phonon-mediated superconductor.

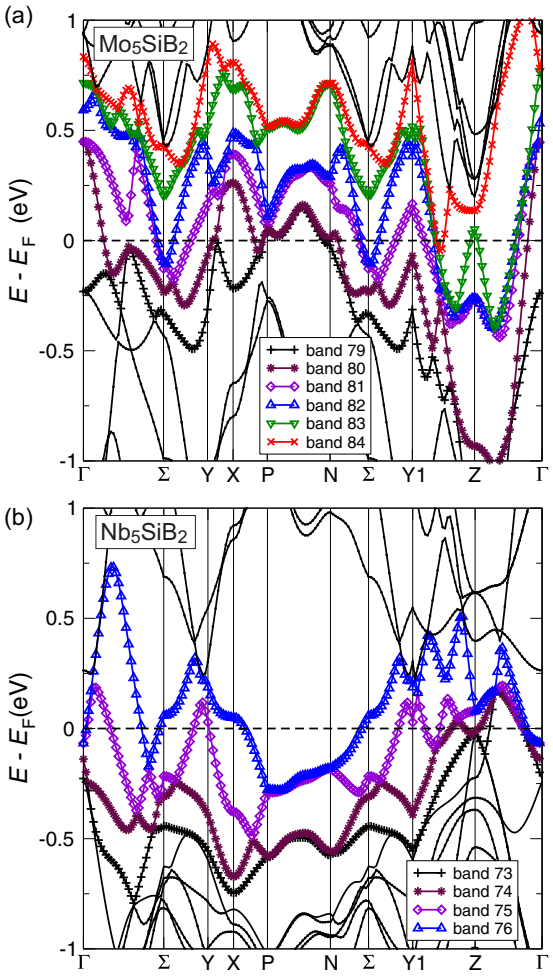

FIG. 7. The calculated band structures for (a) Mo_5SiB_2 and (b) Nb_5SiB_2. Note the multiple bands crossing E_F in each case.

ACKNOWLEDGMENTS

Research was sponsored by the U.S. Department of Energy, Office of Science, Basic Energy Sciences, Materials Sciences and Engineering Division (M.A.M. and D.S.P., synthesis of samples with varying stoichiometry, experimental characterization, theory, and analysis). In addition, M.A.M. acknowledges support for the initial synthesis of the material from U.S. Department of Energy, Office of Energy Efficiency and Renewable Energy, Vehicle Technologies Office, Propulsion Materials Program. The authors thank B. C. Sales and J. Q. Yan for helpful discussions throughout the course of this work.

APPENDIX

1. Electronic structure of Mo_5SiB_2 and Nb_5SiB_2

Figure 7 shows results from first-principles calculations for the superconductors Mo_5SiB_2 and Nb_5SiB_2, isostructural

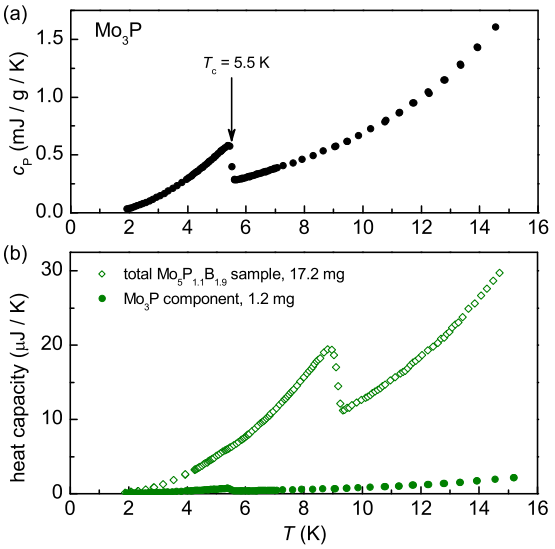

FIG. 8. (a) The measured specific-heat capacity for Mo_3P. (b) Comparison of the total measured heat capacity of the $Mo_5P_{1.1}B_{1.9}$ sample and the calculated contribution from the Mo_3P impurity.

to Mo_5PB_2. These calculations were also carried out using the LAPW method, with an RK_{max} of 7.0 and all internal coordinates relaxed, and approximately 1000 k points in the full Brillouin zone used for all calculations; spin-orbit coupling was not included. As is apparent, both these compounds have multiple bands cutting the Fermi level, with six such bands for Mo_5SiB_2 and four for Nb_5SiB_2. This is indicative of a potential multiband superconductivity in these materials, although definitive resolution of this issue would require further investigation.

2. Heat capacity of Mo_3P

Results of low-temperature heat-capacity measurements on a polycrystalline sample of Mo_3P are shown in Fig. 8(a). The sample was prepared by reacting hydrogen-reduced Mo powder with red phosphorus pieces in an evacuated silica ampoule at 850 °C, then pelletizing the product and firing again at 1150 °C. These data were used to calculate the Mo_3P contribution to the measured heat capacity of the $Mo_5P_{1.1}B_{1.9}$ sample. Figure 8(b) shows the total heat capacity measured from the $Mo_5P_{1.1}B_{1.9}$ sample with a total mass of 17.2 mg. Using the x-ray-diffraction determined concentration of 7 wt % Mo_3P, the heat capacity of the Mo_3P component (1.2 mg), was determined, and is also shown in the figure. These datasets were subtracted using OriginPro to determine the heat capacity of 15 mg of $Mo_5P_{1.1}B_{1.9}$, which is shown in Fig. 4.

[1] P. Villars and K. Cenzual, *Pearson's Crystal Data - Crystal Structure Database for Inorganic Compounds, Release 2013/14* (ASM International, Materials Park, OH, 2013/14).

[2] D. M. de Almeida, C. Bormio-Nunes, C. A. Nunes, A. A. Coelho, and G. C. Coelho, J. Magn. Magn. Mater. **321**, 2578 (2009).

[3] Z. G. Xie, D. Y. Geng, and Z. D. Zhang, Appl. Phys. Lett. **97** (2010).

[4] A. M. Blanc, E. Fruchart, and R. Fruchart, Ann. Chim. **2**, 251 (1967).

[5] R. Wäppling, T. Ericsson, L. Häggström, and Y. Andersson, J. Phys. Colloq. **37**, C6-591 (1976).

[6] M. A. McGuire and D. S. Parker, J. Appl. Phys. **118**, 163903 (2015).

[7] T. N. Lamichhane, V. Taufour, S. Thimmaiahb, D. S. Parker, S. L. Budko, and P. C. Canfield, J. Magn. Magn. Mater. **401**, 525 (2016).

[8] P. Pesliev, G. Gyurov, and R. Soyanchev, Izv. Khim. **19**, 267 (1986).

[9] A. J. S. Machado, A. M. S. Costa, C. A. Nunes, C. A. M. Dos Santos, T. Grant, and Z. Fisk, Solid State Commun. **151**, 1455 (2011).

[10] M. Fukuma, K. Kawashima, M. Maruyama, and J. Akimitsu, J. Phys. Soc. Jpn. **80**, 024702 (2011).

[11] H. Tagaki, M. Nohara, and R. J. Cava, Physica B **237–238**, 292 (1997).

[12] J. Nagamatsu, N. Nakagawa, T. Muranaka, Y. Zenitani, and J. Akimitsu, Nature (London) **410**, 63 (2001).

[13] S. Lebégue, Z. P. Yin, and W. E. Pickett, New. J. Phys. **11**, 025004 (2009).

[14] I. I. Mazin and V. P. Antropov, Physica C **385**, 49 (2003).

[15] K. Ihara, K. Ito, K. Tanaka, and M. Yamaguchi, Mater. Sci. Eng. A **329–331**, 222 (2002).

[16] P. C. Canfield and Z. Fisk, Philos. Mag. B **65**, 1117 (1992).

[17] M. G. Kanatzidis, R. Pöttgen, and W. Jietschko, Angew. Chem. Int. Ed. **44**, 6996 (2005).

[18] J. Rodriguez-Carvajal, FullProf.2k, version 5.30, March 2012.

[19] S. Riegel and G. Weber, J. Phys. E **19**, 790 (1986).

[20] P. Blaha, K. Schwarz, G. Madsen, D. Kvasnicka, and J. Luitz, WIEN2k, An Augmented Plane Wave + Local Orbitals Program for Calculating Crystal Properties, edited by K. Schwarz (Technische Universität Wien, Austria, 2001).

[21] J. P. Perdew, K. Burke, and M. Ernzerhof, Phys. Rev. Lett. **77**, 3865 (1996).

[22] A. Brauner, C. A. Nunes, A. D. Bortolozo, G. Rodrigues, and A. J. S. Machado, Solid State Commun. **149**, 467 (2009).

[23] L. Häggström, R. Wäppling, T. Ericsson, Y. Andersson, and S. Rundqvist, J. Solid State Chem. **13**, 84 (1975).

[24] C. J. Rawn, J. H. Schneibel, C. M. Hoffmann, and C. R. Hubbard, Intermetallics **9**, 209 (2001).

[25] M. Fukuma, K. Kawashima, and J. Akimitsu, J. Phys.: Conf. Ser. **391**, 012090 (2012).

[26] K. Ito, T. Hayashi, and H. Nakamura, Intermetallics **12**, 443 (2004).

[27] Z. Fisk and G. W. Webb, Phys. Rev. Lett. **36**, 1084 (1976).

[28] S. Riegel and G. Weber, Prog. Semicond. **4**, 237 (1960).

[29] N. F. Mott, *Metal-Insulator Transitions* (Taylor and Francis, London, 1974).

[30] M. Gurvitch, Phys. Rev. B **24**, 7404 (1981).

[31] S. L. Bud'ko, C. Petrovic, G. Lapertot, C. E. Cunningham, P. C. Canfield, M.-H. Jung, and A. H. Lacerda, Phys. Rev. B **63**, 220503(R) (2001).

[32] F. Hunte, J. Jaroszynski, A. Gurevich, D. C. Larbalestier, R. Jin, A. S. Sefat, M. A. McGuire, B. C. Sales, D. K. Christen, and D. Mandrus, Nature (London) **453**, 903 (2008).
[33] S. V. Shulga, S.-L. Drechsler, G. Fuchs, K.-H. Müller, K. Winzer, M. Heinecke, and K. Krug, Phys. Rev. Lett. **80**, 1730 (1998).
[34] H. Suderow, V. G. Tissen, J. P. Brison, J. L. Martínez, and S. Vieira, Phys. Rev. Lett. **95**, 117006 (2005).
[35] V. G. Tissen, M. R. Osorio, J. P. Brison, N. M. Nemes, M. García-Hernández, L. Cario, P. Rodière, S. Vieira, and H. Suderow, Phys. Rev. B **87**, 134502 (2013).
[36] H. Wang, C. Dong, Q. Mao, R. Khan, X. Zhou, C. Li, B. Chen, J. Yang, Q. Su, and M. Fang, Phys. Rev. Lett. **111**, 207001 (2013).
[37] B. T. Matthias, E. Corenzwit, and C. E. Miller, Phys. Rev. **93**, 1415 (1954).
[38] R. D. Blaugher, J. K. Hulm, and P. N. Yocom, J. Phys. Chem. Solids **26**, 2037 (1965).
[39] I. Shirotani, M. Takaya, I. Kaneko, C. Sekine, and T. Yagi, Physica C **357–360**, 329 (2001).
[40] J. F. Janak, Phys. Rev. B **16**, 255 (1977).
[41] J. P. Carbotte, Rev. Mod. Phys. **62**, 1027 (1990).
[42] D. J. Van Harlingen, Rev. Mod. Phys. **67**, 515 (1995).
[43] J. D. Fletcher, A. Serafin, L. Malone, J. G. Analytis, J.-H. Chu, A. S. Erickson, I. R. Fisher, and A. Carrington, Phys. Rev. Lett. **102**, 147001 (2009).
[44] C. W. Hicks, T. M. Lippman, M. E. Huber, J. G. Analytis, J.-H. Chu, A. S. Erickson, I. R. Fisher, and K. A. Moler, Phys. Rev. Lett. **103**, 127003 (2009).
[45] H. Won and K. Maki, Phys. Rev. B **49**, 1397 (1994).
[46] A. Y. Liu, I. I. Mazin, and J. Kortus, Phys. Rev. Lett. **87**, 087005 (2001).
[47] F. Bouquet, R. A. Fisher, N. E. Phillips, D. G. Hinks, and J. D. Jorgensen, Phys. Rev. Lett. **87**, 047001 (2001).
[48] J. Daams and J. P. Carbotte, J. Low Temp. Phys. **40**, 135 (1980).